Biochimica et Biophysica Acta 1840 (2014) 1–9

Contents lists available at ScienceDirect

Biochimica et Biophysica Acta

journal homepage: www.elsevier.com/locate/bbagen

Interplay between autophagy and apoptosis mediated by copper oxide nanoparticles in human breast cancer cells MCF7

Dipranjan Laha [a], Arindam Pramanik [a], Jyotirindra Maity [a], Ananda Mukherjee [c], Panchanan Pramanik [b], Aparna Laskar [d], Parimal Karmakar [a,*]

[a] Department of Life Science and Biotechnology, Jadavpur University, Kolkata, 700 032, India
[b] Department of Chemistry, Indian Institute of Technology, Kharagpur 721302, India
[c] Department of Cell and Molecular Biology, University of Rhode Island, Kingston, RI 02881, USA
[d] CSIR-Indian Institute of Chemical Biology, Kolkata 700032, India

ARTICLE INFO

Article history:
Received 19 February 2013
Received in revised form 10 August 2013
Accepted 13 August 2013
Available online 17 August 2013

Keywords:
Copper oxide nanoparticle
Autophagy
Apoptosis
Small interfering RNA

ABSTRACT

Background: Metal oxide nanoparticles are well known to generate oxidative stress and deregulate normal cellular activities. Among these, transition metals copper oxide nanoparticles (CuO NPs) are more compelling than others and able to modulate different cellular responses.
Methods: In this work, we have synthesized and characterized CuO NPs by various biophysical methods. These CuO NPs (~30 nm) induce autophagy in human breast cancer cell line, MCF7 in a time- and dose-dependent manner. Cellular autophagy was tested by MDC staining, induction of green fluorescent protein-light chain 3 (GFP-LC3B) foci by confocal microscopy, transfection of pBABE-puro mCherry-EGFP-LC3B plasmid and Western blotting of autophagy marker proteins LC3B, beclin1 and ATG5. Further, inhibition of autophagy by 3-MA decreased LD_{50} doses of CuO NPs. Such cell death was associated with the induction of apoptosis as revealed by FACS analysis, cleavage of PARP, de-phosphorylation of Bad and increased cleavage product of caspase 3. siRNA mediated inhibition of autophagy related gene beclin1 also demonstrated similar results. Finally induction of apoptosis by 3-MA in CuO NP treated cells was observed by TEM.
Results: This study indicates that CuO NPs are a potent inducer of autophagy which may be a cellular defense against the CuO NP mediated toxicity and inhibition of autophagy switches the cellular response into apoptosis.
Conclusions: A combination of CuO NPs with the autophagy inhibitor is essential to induce apoptosis in breast cancer cells.
General significance: CuO NP induced autophagy is a survival strategy of MCF7 cells and inhibition of autophagy renders cellular fate to apoptosis.

1. Introduction

Nanotechnology offers unique approaches to detect and modulate a variety of biological processes that occur at the nanometer scale and is expected to have a revolutionary impact on biology and medicine [1]. Metal based nanoparticles are showing great prospect as antibacterial agents, in medicine, imaging and drug delivery [2–4]. Thus, different aspects of nanomaterials that may interfere with toxicity (e.g. size, shape, solubility, aggregation and optical features) have been addressed [5–7].

In addition to these applications, metal nanoparticles are considered to interfere with different other biological processes such as autophagy induction and angiogenesis [8–10]. Importantly, autophagy is closely involved in the etiology of many important human diseases including neurodegenerative and metabolic disorders [11,12]. Nowadays, autophagy is becoming an important area in cell biology research associated with cell survival, cell death, cell metabolism, development, aging, infection and immunity [13–18]. Autophagy can be induced by various stimuli, including starvation, cytokines, caspase inhibition and chemical reagents such as rapamycin [19,20]. Nanoparticles have been recently acknowledged as a novel class of materials having the capability to induce autophagy. Different nanomaterials like quantum dots (QD), nanowires and more recently rare earth oxides are reported to induce autophagy in different cell types [21,22]. Nanomaterials may directly have an effect on autophagy dependent signaling pathways by perturbing the expression of related genes. Induction of autophagy in human fibroblasts by gold nanoparticles is associated with the up-regulation of autophagy proteins LC3B and ATG7 [23]. Recently, it has been reported that cationic PAMAM dendrimers and carboxylated carbon nanotubes induce autophagy in human lung adenocarcinoma cells [24,25]. Cytotoxicity

Abbreviations: NAC, N-acetyl cysteine; MDC, monodansylcadaverine; 3-MA, 3-methyladenine; mM, milli molar

* Corresponding author at: Department of Life Science & Biotechnology, Jadavpur University, Kolkata, West Bengal, India. Tel.: +91 3324146710; fax: +91 3324137121.
E-mail address: pkarmakar_28@yahoo.co.in (P. Karmakar).

0304-4165/$ – see front matter © 2013 Elsevier B.V. All rights reserved.
http://dx.doi.org/10.1016/j.bbagen.2013.08.011

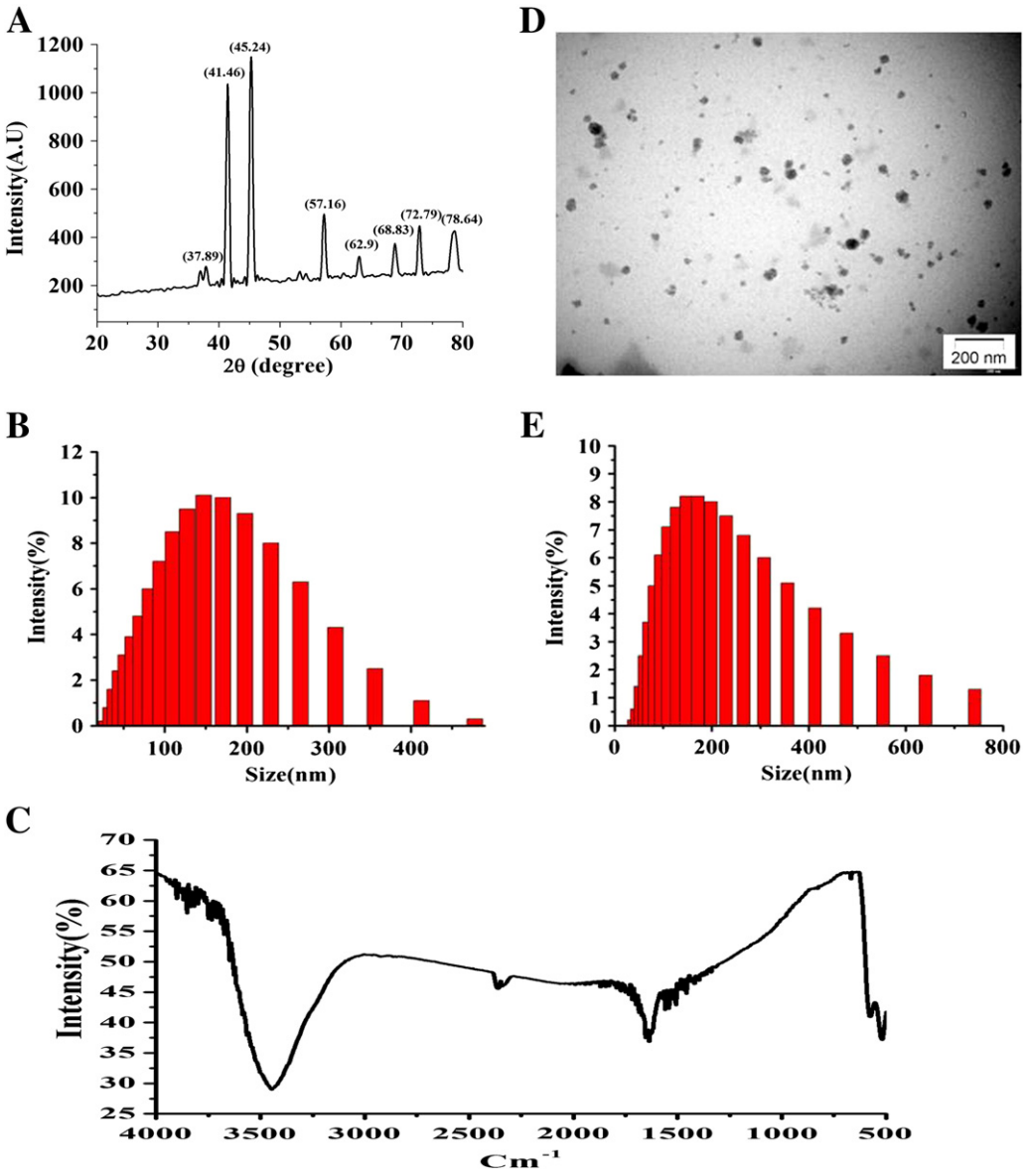

Fig. 1. Physical characterization of CuO NPs; (A) X-ray diffraction patterns; (B, E) size distribution study by DLS in ex vivo and water respectively; (D) transmission electron microscopic (TEM) image of CuO NPs; (C) Fourier transform infrared spectroscopy of CuO NP study.

associated with dendrimer or carbon nanotube treated lung cancer cells was blocked by 3-MA or knockdown of the autophagy gene ATG6, suggesting the involvement of the autophagy pathway in cytotoxicity. On the other hand, it was suggested that autophagy plays a cytoprotective role in response to toxicity exerted by titanium dioxide nanoparticles. However, the exact role of autophagy in response to metal oxide nanoparticles mediated toxicity is not well understood.

Table 1
Characteristic of CuO NPs.

Primary size	Hydrodynamic diameter			Zeta potential, mV		
TEM	Ex vivo, nm	Water, nm	Morphology (TEM)	Ex vivo	Water (pH 6.1)	pDi[a]
30 nm ± 3.5	310	235	Spherical	−17.2	−13.1	0.231

[a] Polydispersity index.

CuO NPs have great interest due to their high redox cycling property and exert cytotoxicity on different cells via oxidative stress. In our study, we have synthesized CuO NPs and physical characterization was done by transmission electron microscopy (TEM), dynamic light scattering (DLS), X-ray diffraction (XRD), and Fourier transform infrared spectroscopy (FTIR). CuO NPs induced autophagy in MCF7 cells in a dose- and time-dependent fashion. Inhibition of autophagy resulted induction of apoptosis suggesting autophagy may be a survival strategy for the MCF7 cells in response to oxidative stress induced by CuO NPs.

2. Materials and methods

2.1. Materials

In this study all chemicals of analytical grade were used. Copper acetate, sodium hydroxide, acetic acid, and N-acetylcysteine were

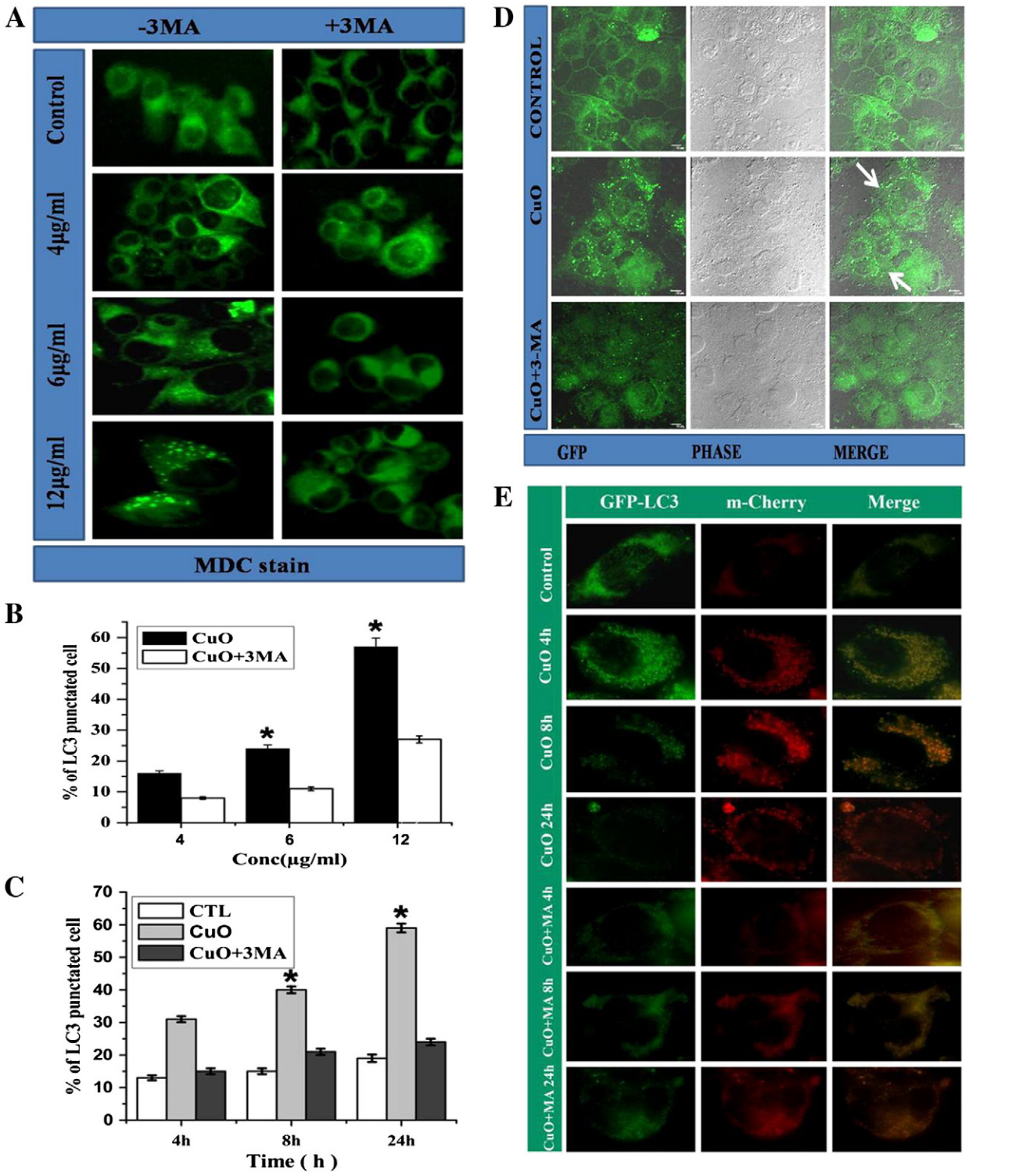

Fig. 2. CuO NPs induce autophagy in MCF7 cells. (A) To evaluate autophagic vacuoles, MCF7cells were treated with different concentrations of CuO NPs in the presence or absence of autophagy inhibitor 3-MA and stained with MDC; (B) percentage of LC3 punctated cells treated with different concentrations of CuO NPs for 24 h; (C) different times of incubation with 12 µg/ml CuO NPs; (D) confocal microscopic images of GFP-LC3 transfected MCF7 cells treated with CuO NPs in the presence or absence of autophagy inhibitor; (E) MCF7 cells were transfected with pBABE-puro mCherry-EGFP-LC3B for 16 h then treated with CuO NPs at different time intervals in presence and absence of autophagy inhibitor. EGFP and m-Cherry signals were observed by fluorescence microscopy.

obtained from Merck (Germany). Bovine serum albumin (BSA) was purchased from SRL (India). 3-MA, MDC, propidium iodide, and osmium tetraoxide (OsO_4) were obtained from Sigma-Aldrich (USA), Anti-LC3B, anti-ATG5, anti-beclin1, anti-cleaved caspase-3, anti-PARP and anti-phospho Bad antibodies were purchased from Cell Signaling Technologies (USA). Horseradish peroxidase-conjugated secondary antibodies were obtained from Santa Cruz Biotechnology, USA. The GFP-LC3B plasmid, which encodes a fusion protein of

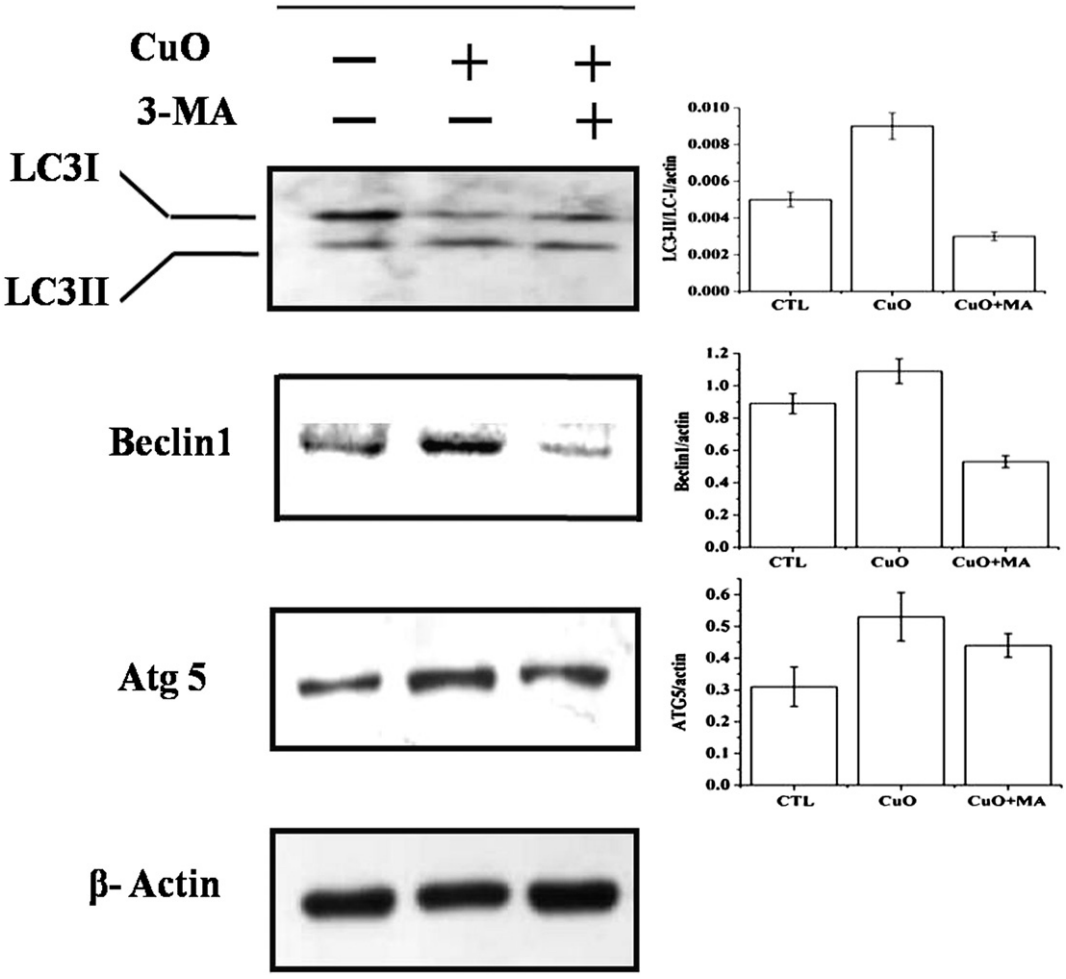

Fig. 3. Western blot analysis of MCF7 cell extracts for LC3B, beclin1 and ATG5 after exposure of cells with CuO NPs for 24 h in the presence or absence of autophagy inhibitor. β-Actin was used as loading control. In the right panel, bar graph represents the quantification data of LC3B, beclin1 and ATG5 in respect to loading control β-actin (arbitrary units, AU; mean ± SD, n = 3; *, $p < 0.05$).

enhanced green fluorescent protein (EGFP) and LC3B plasmid was a kind gift from Prof. Tamatsu Yoshimori (Japan). pBABE-puro mCherry-EGFP-LC3B which encodes a fusion protein (EGFP), m-Cherry and LC3B, was a kind gift from Dr. Jayanta Debnath (Department of Pathology, University of California, San Francisco). siRNA against human beclin1 was purchased from Santa Cruz Biotechnology, USA.

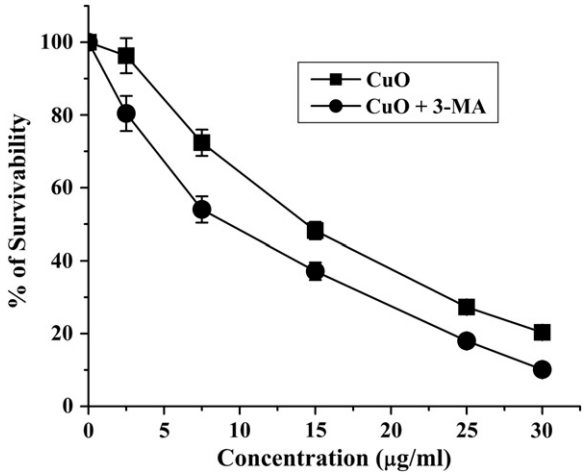

Fig. 4. Cytotoxic effect of CuO NPs on MCF7 cells. Cells were incubated with increasing concentrations of CuO NPs in the presence or absence of 5 mM 3-MA for 24 h and their survivability was assessed by MTT assay. Data represented are means ± SD of three identical experiments made in three replicates. Only 3-MA treated cells almost 93% cells are viable after 24 h.

2.2. Synthesis of CuO NPs

25 mM of copper acetate [$Cu(CH_3COO)_2$] was dissolved in de-ionized water followed by the addition of 50 mM of acetic acid under stirring condition [26]. The solution was heated at boiling temperature at 78 °C. 100 mM of NaOH was added directly to the solution under vigorous stirring. The reaction was performed for 1 h. Resultant product was collected by centrifugation. Finally it was dried at room temperature.

2.3. Physical characterization of CuO NPs

The phase formation and crystallographic state of CuO NPs were determined by XRD with an Expert Pro (Phillips) X-ray diffractometer using CoKα radiation (α = 0.178897 nm). Samples were scanned from 20° to 80° of 2θ increment at 0.04° with 2 s counting time. CuO NPs were dispersed in de-ionized water to form a diluted suspension of 0.5 mg/ml using sonicator for 30 min. After the dispersion of the particles in the water, particle size was analyzed by Brookhaven 90 plus particle size analyzer (DLS). The particle size and nanostructure were studied by high-resolution transmission electron microscopy

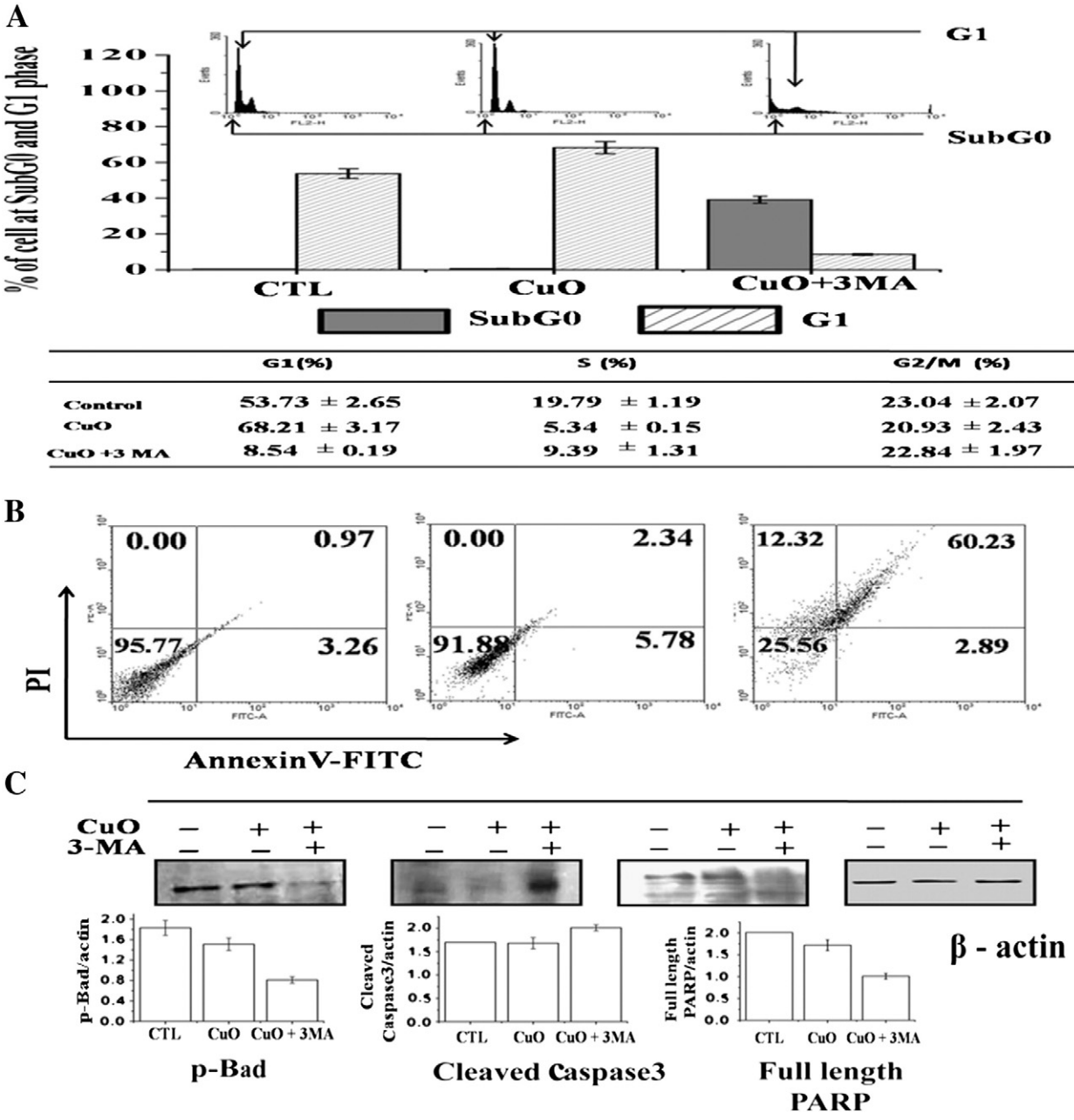

	G1(%)	S (%)	G2/M (%)
Control	53.73 ± 2.65	19.79 ± 1.19	23.04 ± 2.07
CuO	68.21 ± 3.17	5.34 ± 0.15	20.93 ± 2.43
CuO +3 MA	8.54 ± 0.19	9.39 ± 1.31	22.84 ± 1.97

Fig. 5. (A) Flow cytometric analysis of cell-cycle distribution of MCF7 cells, illustrating the effect of CuO NPs (12 μg/ml) in the presence and absence of 3-MA. Cell cycle phase distribution is given on the top of each bar; (B) dot plot of Annexin V-FITC/PI for evaluation of apoptosis in MCF7 cells treated with CuO NPs (12 μg/ml) in the presence and absence of 3-MA. (C) Western blot analysis of apoptosis marker protein in the MCF7 cell extract after the cell was treated with CuO NPs (12 μg/ml) in the presence and absence of 3-MA. In bottom panel corresponding quantification data analysis of these proteins with respect to loading control β-actin is represented (arbitrary units, AU; mean ± SD, n = 3; *, $p < 0.05$).

JEOL 3010 (HRTEM), Japan operating at 200 keV. Presence of surface functional groups was investigated by FTIR spectroscopy (Thermo Nicolet Nexus FTIR, model 870).

2.4. Cell lines, culture condition and treatments

Human breast cancer cells MCF7 were cultured in RPMI-1640 media supplemented with 10% FBS and 100 U ml^{-1} penicillin–streptomycin at 5% CO_2 at 37 °C. At 85% confluence, cells were harvested and sub-cultured according to experimental requirements. Cells were seeded for 24 h prior to the treatment with CuO NPs. All the treatments were performed at 37 °C at a density allowing exponential cell growth.

2.5. Acidic vesicular organelles labeled by monodansylcadaverine (MDC)

MCF7 cells (2.4×10^4) were seeded into 35 mm plates. After 24 h incubation, CuO NPs were added with an increasing concentration in the presence or absence of 3-MA for different time periods [27]. The cells were then incubated with 50 mmol/l MDC at 37 °C for 15 min and washed with 1× PBS three times with 5 min interval. Finally, the cells were observed under a fluorescence microscope (Leica DM 2500).

2.6. Green fluorescent protein-light chain 3 (GFP-LC3B) plasmid transfection

MCF7 cells were transfected with 1 μg of GFP-LC3B plasmid using FuGENE as per the manufacturer's instructions (Roche). After 16 h,

cells were treated with CuO NPs at 12 μg/ml for 24 h. Finally these cells were washed, then mounted on glass slides and observed under a confocal microscope (Olympus ix81) [27].

2.7. Autophagic flux measurement pBABE-puro mCherry-EGFP-LC3B plasmid transfection

To monitor autophagic flux, MCF7 cells were transfected with pBABE-puro mCherry-EGFP-LC3B using FuGENE as per the manufacturer's instructions (Roche). After 16 h, cells were treated with CuO NPs at 12 μg/ml for different times with or without inhibitor. Cells were washed and mounted on glass slides. Finally, cells were monitored over time for EGFP and m-Cherry under a fluorescence microscope (Leica DM 2500) [28].

2.8. Western blotting assay

The cells were lysed in 100 ml pre-cooled lysis buffer containing 0.5% Triton X100, 100 mM Tris–HCl, 150 mM NaCl, and 0.1 U/ml aprotinin for 30 min on ice and centrifuged at 12,000 *g* for 2 min. The supernatant was collected and protein concentration was estimated using Bradford's reagent with bovine serum albumin (BSA) as standard control. The supernatant was then mixed with double volume of sample buffer (62.5 mM Tris, pH 6.8, 2% SDS, 5% mercaptoethanol, 1% bromophenol blue and 25% glycerol) and boiled for 5 min. On a 10% SDS-PAGE, 20 μg protein was separated. Proteins were then transferred to a polyvinylidene-difluoride (PVDF) membrane (Bio-Rad) [29]. The membrane was blocked using 5% skimmed milk for 1 h at room temperature and incubated overnight at 4 °C with primary antibody. After washing six times with TBST, 10 min each, the membrane was incubated in the appropriate HRP-conjugated secondary antibody (diluted 1:2000 in TBST) at room temperature for 2 h. The membrane was then incubated with enhanced chemiluminescence reagent (ECL) solution for 3 min. Visualization of the immunolabelled bands was carried out by autoradiography.

2.9. MTT assay for cell viability

The inhibition of cell growth was measured by MTT assay as described previously [30]. In brief, cells were seeded in 96 well plates at 1×10^4 cells per well and exposed to CuO NPs at different concentrations for 24 h. After incubation, cells were washed twice with PBS and incubated with MTT solution (450 μg/ml) for 3–4 h at 37 °C. The resulting formazan crystals were dissolved in a MTT solubilization buffer and the absorbances were measured at 570 nm by using a microplate reader (Biotek, USA). Each point was assessed in triplicate.

2.10. Cell cycle analysis

For cell cycle analysis, 1×10^6 cells/ml were treated with CuO NPs in the presence or absence of 3-MA at LD_{50} dose. After 24 h incubation, the cells were washed with 1× PBS and fixed with chilled 80% ethanol and kept for 2 h at 4 °C. Prior to stain with 50 μg/ml propidium iodide (PI, Sigma), the cells were incubated for 1 h with 100 μg/ml of DNAse free

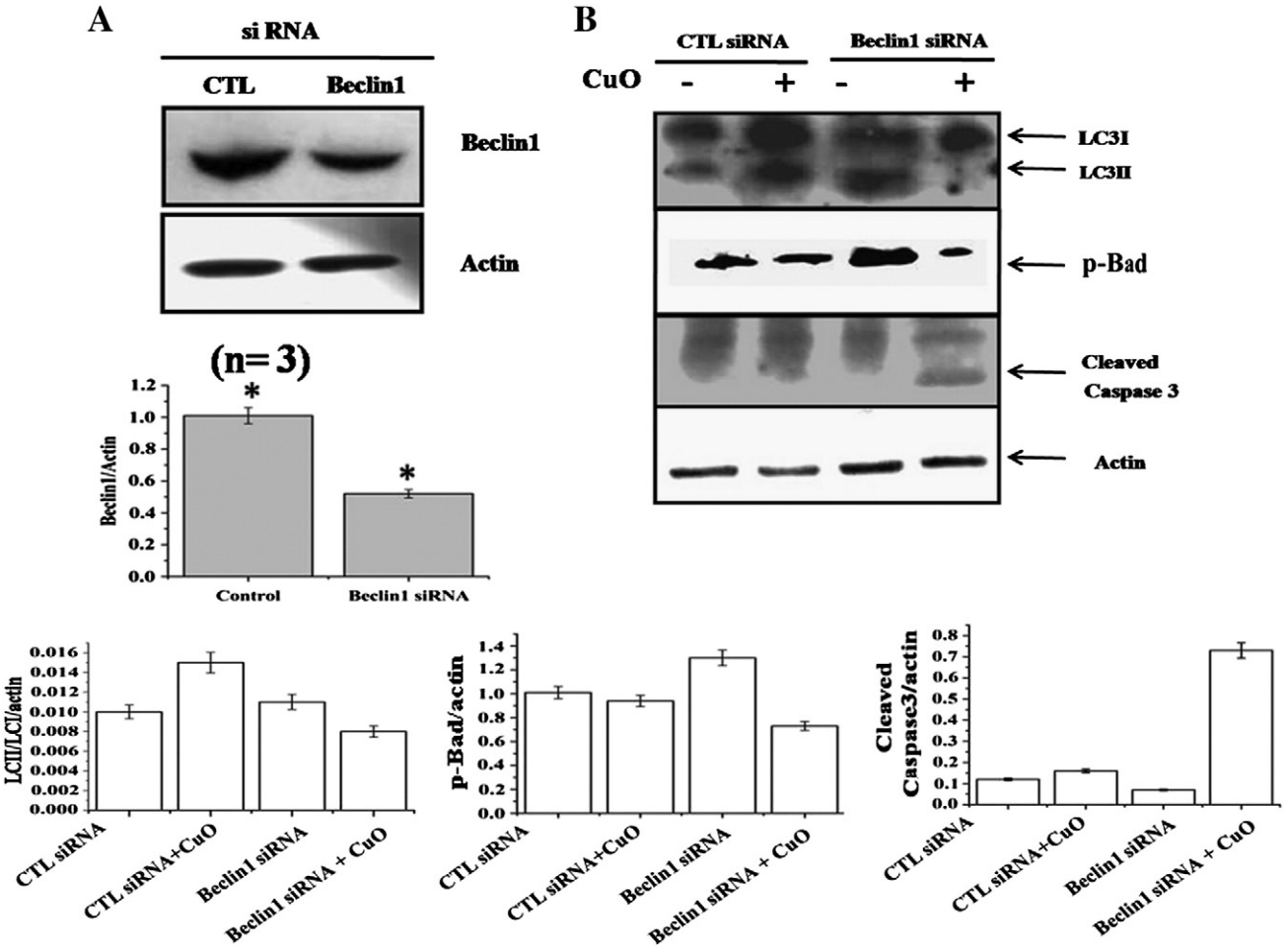

Fig. 6. (A) Western blotting analysis of the expression of beclin1 in beclin1 siRNA and control siRNA transfected cells. Bottom panel shows the representation of the quantitative analysis of these proteins. (B) Expression of autophagic marker (LC3B) and apoptotic marker (p-Bad and cleaved caspase 3) in beclin1 siRNA and control siRNA transfected cell in presence and absence of CuO NPs. Bottom panel shows the representation of the quantitative analysis of these proteins.

RNAse A (SRL, India) at 37 °C [31]. The cell cycle was analyzed with a Becton Dickinson (FACS Calibur) flow cytometer, equipped with an air-cooled 20 mW argon laser. 25,000 events were counted at each data point.

2.11. Apoptosis measurement by Annexin V-FITC staining

The method for analysis cellular apoptosis was described elsewhere [31]. In brief, both control and CuO NP treated cells were incubated for 24 h in a 37 °C, 5% CO_2 incubator in the presence or absence of 3-MA. Following the incubation, the cells were washed twice with 1× PBS. After that, the cells were resuspended in 1× Annexin binding buffer. 500 μl of each cell suspension was added to a plastic 12 × 75 mm FACS tube and 2 μg/ml of Annexin V-FITC (sigma) and 0.5 μg/ml of propidium iodide (sigma) were added to each cell suspension. The tubes were incubated at room temperature for 15 min at dark. Finally, the fluorescence of cells was immediately determined by Becton Dickinson (FACS Calibur) flow cytometer.

2.12. Small interfering RNA (siRNA) mediated silencing of beclin1

Cells were transfected with beclin1 siRNA (50-CAGUUUGGCACAA UCAAUATT-30) or scrambled siRNA (50-UUCUCCGAACGUGUCACGU TT-30, Santa Cruz, CA, USA) using Santa Cruz transfection reagent according to the manufacturer's instructions. After 24 h, knockdown efficacy was determined by Western blotting with anti-beclin1 antibody.

2.13. Transmission electron microscopy (TEM)

MCF7 cells were treated with CuO NPs (12 μg/ml) in the presence or absence of autophagy inhibitor 3-MA for 24 h. Cells were then collected and prefixed with 2.5% glutaraldehyde. These cells were then post fixed with 1% osmium tetraoxide for 1 h, dehydrated by increasing concentrations of acetone and then gradually infiltrated with epoxy resin; ultrathin sections (50–70 nm) were cut using a Leica Ultramicrotome EM UC6 and contrasted using 1% aqueous uranyl acetate for 5 min and lead citrate in a CO_2-depleted atmosphere for 4 min. A FEI TECNAI G^2 Spirit BioTWIN electron microscope was used to study the sections in 100 kV.

2.14. Statistical analysis

A Student's *t*-test was used to calculate the statistical significance of the changes. In all cases, the p value less than 0.05 was considered as statistically significant. Data analysis was performed using the Origin Pro v. 8 software (Origin Lab).

3. Results

We first characterized the purity of CuO NPs by XRD. The XRD pattern of CuO NPs was compared and interpreted with standard data of the JCPDS file (JCPDS International Center for Diffraction Data, 1991). All possible peaks of CuO NPs are observed, which indicates the polycrystalline nature of the product. Fig. 1A shows the XRD pattern of CuO NPs, the characteristic peaks at $2\theta = 37.89°$, 41.46°, 45.24°, 54.20°, 57.16°, 62.9°, 68.83°,72.79° and 78.64° which are marked respectively by their indices in agreement with JCPDS card nos 80–1916. The hydrodynamic size of CuO NPs was measured by DLS. Table 1 summarizes the physical characterization of these NPs. Fig. 1B and E represents the frequency of size distribution of these NPs in de-ionized water and RPMI 1640 respectively. TEM analysis revealed that these particles have an almost spherical geometry with mean diameter of 30 nm ± 3.5 (Fig. 1D). FTIR spectroscopy is a useful tool to understand the functional group of any organic molecule. Fig. 1C shows that the pure CuO NPs (a) exhibited strong band at 517 cm^{-1} and 585 cm^{-1}, characteristic of the Cu – O bond and the broad band around 3440 cm^{-1}, which indicates the presence of – OH groups on the nanoparticle's surface. Next, we carried out experiments

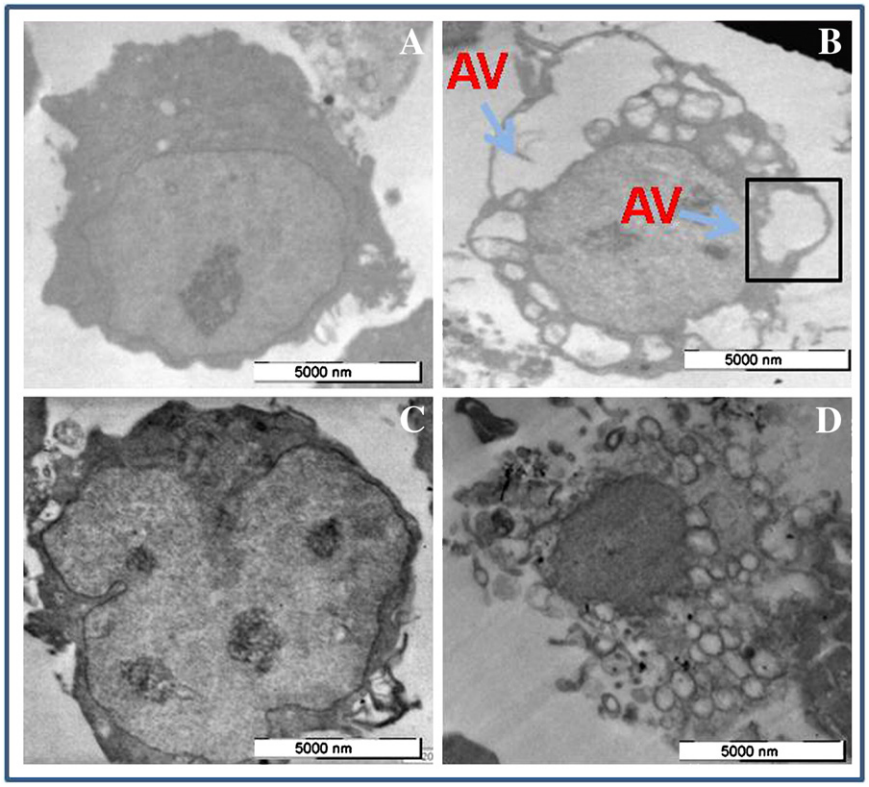

Fig. 7. Electron microscopic image of MCF7 cell. (A) Control; (B) 12 μg/ml CuO NP treated cells; both (C) and (D) represent MCF7 cells treated with CuO NPs in the presence of 3-MA to demonstrate early and late apoptosis. Arrow indicates the autophagic vacuoles (AV) in CuO NP treated cells.

to investigate the effect of these synthesized NPs on human breast cancer cell line MCF7. In order to determine the role of nanoparticles in autophagy induction, MCF7 cells were incubated with CuO NPs at different concentrations (4, 6, 12 μg/ml respectively). Cells were then seen under fluorescence microscope after MDC staining. Fig. 2A shows that CuO NPs induce autophagy in MCF7 cells in a dose dependent manner. When CuO NPs were treated in the presence of 3-MA, the amount of cells undergoing autophagy decreased (Fig. 2A). Fig. 2B represents a quantitative analysis of dose dependent autophagy induction. From Fig. 2C it is also seen that CuO NPs induced autophagy in a time dependent manner. One step further, we have used confocal microscope to analyze GFP-LC3 foci in CuO NP treated GFP-LC3B plasmid transfected cells in the presence or absence of the autophagy inhibitor (Fig. 2D). Thus, the exposure of these nanoparticles leads to induction of autophagy in a time- and dose-dependent manner in MCF7 cells (Fig. 2A, B and C). Next, we used a pH-sensitive, double tagged mCherry-GFP-LC3 (dtLC3) reporter to determine the fusion efficiency of autophagosome with lysosome. As GFP but not Cherry fluorescence is lost in acidic compartments, mCherry-GFP-LC3 labelled non-acidic autophagosomes appear as yellow/orange fluorescence (positive for both green and red), but acidic autophagolysosomes as red fluorescence only. As seen in Fig. 2E, up to 8 h orange fluorescence of the foci was observed but at 24 h green fluorescence diminished indicating fusion of autophagosome with lysosome. Presence of autophagy inhibitor abolished the typical punctated foci of LC3. In light of these findings, we additionally performed Western blotting of the protein extracts from the cells to probe for autophagy marker proteins, like microtubule-associated protein 1 light chain 3 (MAP-LC3B), ATG5, and beclin1. Fig. 3 shows that the conjugated MAP-LC3-II protein level of the cells was significantly higher than the control which correlates with autophagosome formation. Also beclin1 and ATG5 increase in CuO NP treated cells. Quantitative analysis of the protein compared to β-actin is shown in the right panel where β-actin was used as loading control.

Given that induction of autophagy by CuO NPs in MCF7 cells is reduced in the presence of 3-MA, we then explored the fate of the cells after autophagy inhibition. Consequently, we have performed a MTT assay with different concentration of CuO NPs in the presence or absence of 3-MA. As seen in Fig. 4, the amount of cell survival decreases in all the concentrations of CuO NP treated cells when 3-MA was present. We first analyzed the cell cycle of nanoparticle treated cells by FACS. As seen in Fig. 5A, when only CuO NPs were treated for 24 h, MCF7 cells are arrested to G1 phase but in the presence of both CuO NPs and 3-MA, the majority of the cells are in sub-G0 indicating, induction of apoptosis. To confirm the apoptosis in MCF7 cells, we also labeled the cells with Annexin V-FITC followed by FACS analysis and found majority of cells were in a late apoptosis stage when CuO NPs were treated in the presence of 3-MA (Fig. 5B). To further establish this we also immunoblotted the cell extract with antibodies specific for apoptosis marker proteins. As seen in Fig. 5C amount of Bad phosphorylation reduced, PARP is cleaved and increase in caspase 3 cleaved product when autophagy was inhibited with 3-MA in CuO NP treated cells. Further, induction of apoptosis was observed when autophagy related gene beclin1 was knocked down in MCF7 cells (Fig. 6). In Fig. 6A, cell extract was immunoblotted with beclin1 antibody to demonstrate the knockdown of beclin1 compared to scramble siRNA transfected cell extract. Corresponding quantitative analysis of beclin1 compared to β-actin is shown in the bottom. Almost 50–60% knockdown was achieved. When such cells were treated with CuO NPs for 24 h and cell extract was immunoblotted with apoptosis marker antibodies, we obtained almost similar results (Fig. 6B). Knocking down of beclin1 resulted in inhibition of autophagy (LC3 decreases), decrease in phospho Bad and increase in caspase 3 cleavage product. Finally we confirmed our results by TEM. After treatment with CuO NPs (Fig. 7) induction of autophagy vacuoles was observed in MCF7cells. However, when CuO NPs were treated in the presence of 3-MA (Fig. 7C and D) we found shrinkage or fragmented nuclei, an indicator of early or late apoptosis respectively.

4. Discussion

The use of metal based nanoparticles is continuously expanding due to their wide applications and unique physicochemical properties [32,33]. Among several metal oxide nanoparticles, CuO NPs are toxic to a variety of cells and generation of ROS contributes largely for the CuO NP toxicity [34]. However, having potential to participate in cellular redox cycling CuO NPs may also induce other kinds of cellular stresses [35]. In this work, we have synthesized stable monodispersed CuO NPs (diameter ~30 nm, polydispersity ~0.217) and explored the additional role of CuO NPs in human breast cancer cells MCF7. The mechanisms of induction of autophagy are not clear but it seems likely that cellular stress induced by CuO NPs is responsible for the induction of autophagy. Autophagy or cellular self-digestion is a conserved mechanism involved in the degradation of proteins and organelles in the cytoplasm [36]. Even though autophagy primarily serves as a pro-survival mechanism in contexts including nutrient and growth factor deprivation, ER stress and microbial infection, it has been also shown that prolonged and uncontrolled autophagy is involved in cell death. Usually, cellular response to CuO NP induced stress is mostly apoptosis which prompted many researchers to consider the therapeutic potential of CuO NPs [37]. But two recent studies reported that copper complex and CuO NPs induce autophagy in Hela and A549 cells respectively; however the dual role of CuO NPs in autophagy and apoptosis induction in MCF7 cell has not been reported earlier [38,39]. MCF7 cells are usually known as chemoresistance and have the potential to develop strategy in response to cellular stress induced by different chemotherapeutic agents such as adriamycin and paclitaxel [40]. The mechanisms of such chemoresistance nature involve multiple complex biological processes. Recent gene array studies have identified some additional anti-apoptotic candidate proteins, such as the member of the MAPK family, MEK5-BMK/Erk5, which may contribute to anti-apoptotic signaling associated with MCF7 cell [41]. CuO NPs are readily up take by different cells as reported and induce ROS which is essential for the induction of autophagy [42]. Thus while inhibiting ROS by NAC, amount of autophagy in MCF7 cells decreases after CuO NP treatment (data not shown). Thus it is probable that autophagy in MCF7 cells serves as a survival strategy as inhibition of autophagy results in induction of apoptosis. Fine tuning between autophagy and apoptosis induced by nanoparticles or even by other agents is not clearly known but it mainly depends on the types of cell used. Thus, there are several reports where CuO NPs induce apoptosis in different cells [43]. We have demonstrated the formation of autophagy vacuoles by TEM (Fig. 7B) and also confirmed the fusion of autophagosome with lysosome after treatment of CuO NPs. Such fusion increases with time of incubation in CuO NP treated cell (Fig. 2E). Additionally, CuO NPs may interfere with signaling associated with autophagy or induced ER stress which rapidly triggers autophagy. The role of autophagy regulation by the class I PI3K signaling pathway is known; therefore we have used a well-known autophagic inhibitor 3-MA which blocks the phosphoinositide 3-kinase (PI3K) activity [44]. However, there is one report about the dual role of 3-MA [44]. It has been demonstrated that 3-MA can inhibit as well as stimulate autophagy. In our control experiment, we found that 3-MA at a concentration of 3 mM or 5 mM cannot induce autophagy or change cell cycle (see Supplementary Figs. S1 and S2). We have seen that autophagy induced by CuO NPs was successfully inhibited when cells were treated with 3-MA at a concentration of 5 mM. The apparent discrepancy is due to the differences in cell type used. But we have also confirmed our observation with TEM and transfecting cells with beclin1 siRNA (Figs. 7 and 6).

Presence of NAC in CuO NP treated cells resulted in reduced amount of autophagy (data not shown) indicating ROS mediated autophagy induction [45]. Thus taken together, MCF7 cells rapidly uptake CuO

NPs which after entering into the cells produce ROS and perturb different metabolic processes [46]. MCF7 cells having high rate of metabolic demand utilize autophagy pathway to maintain its survival. Inhibition of autophagy triggers the apoptosis pathway for such cells due to rapid accumulation of ROS mediated damages. Thus, inhibition of autophagosome formation with 3-MA or beclin1 siRNA that leads the cells to apoptosis is justified. So, while considering the therapeutic potential of CuO NPs it is necessary to block autophagy.

5. Conclusion

This study shows that CuO NPs induce in vitro growth inhibition and autophagy in MCF7 cells. Collectively, this study indicates that a combination of CuO NPs with autophagy inhibitor is essential to induce apoptosis in breast cancer cells. This approach may be an effective therapeutic strategy, in general, to sensitize chemoresistant cancer cells.

Supplementary data to this article can be found online at http://dx.doi.org/10.1016/j.bbagen.2013.08.011.

Acknowledgements

The authors would like to acknowledge for financial support for this research work the Department of Biotechnology, Government of India (No. BT/PR14661/NNT/28/494/2010). We sincerely acknowledge Dr. Jayanta Debnath (Department of Pathology, University California, San Francisco) for pBABE-puro mCherry-EGFP-LC3B and Prof. Tamatsu Yoshimori (Osaka, Japan) for GFP-LC3 plasmid. We also express sincere thanks to Prof. S. Roy, Director, Indian Institute of Chemical Biology, Kolkata, India, for his permission to use the transmission electron microscope.

References

[1] E.S. Kawasaki, A. Player, Nanotechnology, nanomedicine, and the development of new, effective therapies for cancer, Nanomed Nanotechnol. 2 (2005) 101–109.
[2] A. Pramanik, D. Laha, D. Bhattacharya, P. Pramanik, P. Karmakar, A novel study of antibacterial activity of copper iodide nanoparticle mediated by DNA and membrane damage, Colloids Surfaces B. 96 (2012) 50–55.
[3] Y.H. Kim, D.K. Lee, H.G. Cha, C.W. Kim, Y.S. Kang, Synthesis and characterization of antibacterial Ag–SiO_2 nanocomposite, J. Phys. Chem. C 111 (2007) 3629–3635.
[4] S. Chandra, P. Das, S. Bag, D. Laha, P. Pramanik, Synthesis, functionalization and bioimaging applications of highly fluorescent carbon nanoparticles, Nanoscale 3 (2011) 1533–1540.
[5] Y. Pan, S. Neuss, A. Leifert, M. Fischler, F. Wen, U. Simon, G. Schmid, W. Brandau, W. Jahnen-Dechent, Size-dependent cytotoxicity of gold nanoparticles, Small 11 (2007) 1941–1949.
[6] Y. Guo, J. Zhang, L. Yang, H. Wang, F. Wang, Z. Zheng, Syntheses of amorphous and crystalline cupric sulfide nanoparticles and study on the specific activities on different cells, Chem Comm. 46 (2010) 3493–3495.
[7] A.M. Studera, L.K. Limbacha, L.V. Ducb, F. Krumeichc, E.K. Athanassioua, L.C. Gerbera, H. Mochb, W.J. Starka, Nanoparticle cytotoxicity depends on intracellular solubility: comparison of stabilized copper metal and degradable copper oxide nanoparticles, Toxicol. Lett. 197 (2010) 169–174.
[8] H.A. Ngwa, A. Kanthasamy, Y. Gu, N. Fang, V. Anantharam, A.G. Kanthasamy, Manganese nanoparticle activates mitochondrial dependent apoptotic signaling and autophagy in dopaminergic neuronal cells, Toxicol. Appl. Pharmacol. 256 (2011) 227–240.
[9] R.K. Shukla, V. Sharma, A.K. Pandey, S. Singh, S. Sultana, A. Dhawan, ROS-mediated genotoxicity induced by titanium dioxide nanoparticles in human epidermal cells, Toxicol. in Vitro. 25 (2011) 231–241.
[10] M. Dowding, S. Oommenc, A. Kumar, T.X.T. Sayle, S. Saraf, C.R. Patra, N.E. Vlahakis, D.C. Sayle, W.T. Self, S. Seal, The induction of angiogenesis by cerium oxide nanoparticles through the modulation of oxygen in intracellular environments, Biomaterials 33 (2012) 7746–7755.
[11] S. Das, S. Singh, J.R.A. Nixona, D. Yang, Autophagy failure in Alzheimer's disease-locating the primary defect, Neurobiol. Dis. 43 (2011) 38–45.
[12] H. Nia, J.A. Williamsa, H. Yanga, Y. Shib, J. Fanb, W. Dinga, Targeting autophagy for the treatment of liver diseases, Pharmacol. Res. 66 (2012) 463–474.
[13] Q. Huang, H. Shen, The dual role of poly(ADP-ribose) polymerase-1 in autophagy and necrosis under oxidative stress and DNA damage, Autophagy 5 (2009) 273–276.
[14] H. Shena, P. Codogno, Autophagy is a survival force via suppression of necrotic cell death, Exp. Cell Res. 318 (2012) 1304–1308.
[15] F. Lozya, V. Karantzaa, Autophagy and cancer cell metabolism, Semin. Cell Dev. Biol. 23 (2012) 395–401.
[16] K. Tsuchihara, S. Fujii, H. Esumi, Autophagy and cancer: dynamism of the metabolism of tumor cells and tissues, Cancer Lett. 278 (2009) 130–138.
[17] S. Husseya, L.H. Travassosc, N.L. Jonesa, Autophagy as an emerging dimension to adaptive and innate immunity, Semin. Immunol. 21 (2009) 233–241.
[18] R. Rezzani, A. Stacchiotti, L.F. Rodella, Morphological and biochemical studies on aging and autophagy, Ageing Res. Rev. 11 (2012) 10–31.
[19] H. Yuan, C.N. Perry, C. Huang, E. Iwai-Kanai, R.S. Carreira, C.C. Glembotski, R.A. Gottlieb, LPS-induced autophagy is mediated by oxidative signaling in cardiomyocytes and is associated with cytoprotection, Am. J. Physiol. Heart Circ. Physiol. 296 (2009) 470–479.
[20] C. Cao, T. Subhawong, J.M. Albert, K.W. Kim, L. Geng, K.R. Sekhar, Y. Jin Gi, B. Lu, Inhibition of mammalian target of rapamycin or apoptotic pathway induces autophagy and radiosensitizes PTEN null prostate cancer cells, Cancer Res. 20 (2006) 10040–10047.
[21] S.T. Stern, B.S. Zolnik, C.B. McLeland, J. Clogston, J. Zheng, S.E. McNeil, Induction of autophagy in porcine kidney cells by quantum dots: a common cellular response to nanomaterials? Toxicol. Sci. 106 (2008) 140–152.
[22] N.K. Verma, J. Conroy, P.E. Lyons, J. Coleman, M.P. O'Sullivan, H. Kornfeld, D. Kelleher, Y. Volk, Autophagy induction by silver nanowires: a new aspect in the biocompatibility assessment of nanocomposite thin films, Toxicol. and Applied. Pharmacol. 264 (2012) 451–461.
[23] J.J. Li, D. Hartono, C. Ong, B. Bay, L.L. Yung, Autophagy and oxidative stress associated with gold nanoparticles, Biomaterials 31 (2010) 5996–6003.
[24] C. Li, H. Liu, Y. Sun, H. Wang, F. Guo, S. Rao, J. Deng, Y. Zhang, Y. Miao, C. Guo, J. Meng, X. Chen, L. Li, D. Li, H. Xu, H. Wang, B. Li, C. Jiang, PAMAM nanoparticles promote acute lung injury by inducing autophagic cell death through the Akt–TSC2–mTOR signaling pathway, Moll. cell. bio. 1 (2009) 37–45.
[25] H. Liu, Y. Zhang, N. Yang, Y. Zhang, X. Liu, C. Li, Y. Zhao, Y. Wang, G. Zhang, P. Yang, F. Guo, Y. Sun, C. Jiang, A functionalized single-walled carbon nanotube-induced autophagic cell death in human lung cells through Akt–TSC2–mTOR signaling, Cell Death Differ. 2 (2011) 159.
[26] T. Kida, T. Oka, M. Nagano, Synthesis and application of stable copper oxide nanoparticle suspensions for nanoparticulate film fabrication, J. Am. Ceram. Soc. 90 (2007) 107–110.
[27] N. Mizushima, Methods for monitoring autophagy, Int. J. Biochem. Cell Biol. 36 (2004) 2491–2502.
[28] T. Sun, Y. Yan, Y. Zhao, F. Guo, C. Jiang, Copper oxide nanoparticles induce autophagic cell death in A549 cells, Plosone. 7 (2012) 43442.
[29] S. Pankiv, T.H. Clausen, T. Lamark, A. Brech, J. Bruun, H. Outzen, A. Bjørkøy, T. Johansen, p62/SQSTM1 binds directly to Atg8/LC3 to facilitate degradation of ubiquitinated protein aggregates by autophagy, J. Biol. Chem. 282 (2007) 24131–24145.
[30] M. Jo, T. Kim, D. Seol, J.E. Esplen, K. Dorko, T.R. Billiar, S.C. Strom, Apoptosis induced in normal human hepatocytes by tumor necrosis factor-related apoptosis-inducing ligand, Nat. Med. 6 (2000) 564–567.
[31] L.L. Vindeløv, I.J. Christensen, N.I. Nissen, A detergent-trypsin method for the preparation of nuclei for flow cytometric DNA analysis, Cytometry 5 (1983) 323–327.
[32] M.J. Sweet, A. Chessher, I. Singleton, Metal-based nanoparticles; size, function, and areas for advancement in applied microbiology, Adv. Appl. Microbiol. 80 (2012) 113–142.
[33] I.S. Chekman, Z.R. Ulberg, N.O. Gorchakova, T.Y. Nebesna, T.G. Gruzina, A.O. Priskoka, A.M. Doroshenko, P.V. Simonov, The prospects of medical application of metal-based nanoparticles and nanomaterials, Lik. Sprava 1–2 (2011) 3–21.
[34] B. Fahmy, S.A. Cormier, Copper oxide nanoparticles induce oxidative stress and cytotoxicity in airway epithelial cells, Toxicol. In Vitro 23 (2009) 1365–1371.
[35] B. Levine, D.J. Klionsky, Development by self-digestion: molecular mechanisms and biological functions of autophagy, Dev. Cell 6 (2004) 463–477.
[36] C.N. Hancock, L.H. Stockwin, B. Han, R.D. Divelbiss, J.H. Jun, S.V. Malhotra, M.G. Hollingshead, D.L. Newton, Copper chelate of thiosemicarbazone NSC 689534 induces oxidative/ER stress and inhibits tumor growth in vitro and in vivo, Free Radic. Biol. Med. 50 (2011) 110–121.
[37] Y. Wang, X. Zi, J. Su, H. Zhang, X. Zhang, H. Zhu, J. Li, M. Yin, F. Yang, Y. Hu, Cuprous oxide nanoparticles selectively induce apoptosis of tumor cells, Int. J. Nanomedicine 7 (2012) 2641–2652.
[38] T. Sun, Y. Yan, Y. Zhao, F. Guo, C. Jiang, Copper oxide nanoparticles induce autophagic cell death in A549 cells, PLoS One 7 (2012) 43442.
[39] W. Guo, S. Ye, N. Cao, J. Huang, J. Gao, Q. Chen, ROS-mediated autophagy was involved in cancer cell death induced by novel copper(II) complex, Exp. Toxicol. Pathol. 62 (2010) 577–582.
[40] R. Simstein, M. Burow, A. Parker, C. Weldon, B. Beckman, Apoptosis, chemoresistance, and breast cancer: insights from the MCF-7 cell model system, Exp. Biol. Med. 228 (2003) 995–1003.
[41] L.L. Fu, Y. Yang, H.L. Xu, Y. Cheng, X. Wen, L. Ouyang, J.K. Bao, Y.Q. Wei, B. Liu, Identification of novel caspase/autophagy-related gene switch to cell fate decisions in breast cancers, Cell Prolif. 46 (2013) 67–75.
[42] N. Hanagata, F. Zhuang, S. Connolly, J. Li, N. Ogawa, M. Xu, Molecular responses of human lung epithelial cells to the toxicity of copper oxide nanoparticles inferred from whole genome expression analysis, ACS Nano 5 (2011) 9326–9338.
[43] J. Xu, Z. Li, P. Xu, L. Xiao, Z. Yang, Nanosized copper oxide induces apoptosis through oxidative stress in podocytes, Arch. Toxicol. (2012), http://dx.doi.org/10.1007/s00204-012-0925-0.
[44] Y. Wu, H. Tan, G. Shui, C. Bauvy, Q. Huang, M.R. Wenk, C. Ong, P. Codogno, H. Shen, Dual role of 3-methyladenine in modulation of autophagy via different temporal patterns of inhibition on class I and III phosphoinositide3-kinase, J. Biol. Chem. 14 (2010) 10850–10861.
[45] S. Park, J. Kimb, G. Chi, G. Kimc, Y. Chang, S. Moon, S. Namb, W. Kimh, Y. Yoo, Y.H. Choi, Induction of apoptosis and autophagy by sodium selenite in A549 human lung carcinoma cells through generation of reactive oxygen species, Toxicol. Lett. 212 (2012) 252–261.
[46] M.L. Turski, D.J. Thiele, New roles for copper metabolism in cell proliferation, signaling, and disease, J. Biol. Chem. 284 (2009) 717–721.